Journal of Zhejiang University-SCIENCE A (Applied Physics & Engineering) 2023 24(5):450-464
www.jzus.zju.edu.cn; www.springer.com/journal/11582
E-mail: jzus_a@zju.edu.cn

Research Article
https://doi.org/10.1631/jzus.A2200374

Influence of yaw damper layouts on locomotive lateral dynamics performance: Pareto optimization and parameter analysis

Guang LI[1], Yuan YAO[1]✉, Longjiang SHEN[2], Xiaoxing DENG[2], Wensheng ZHONG[1]

[1]*State Key Laboratory of Traction Power, Southwest Jiaotong University, Chengdu 610031, China*
[2]*Bogie R&D Department of CRRC Zhuzhou Electric Locomotive Co., Ltd., Zhuzhou 412001, China*

Abstract: High-speed locomotives are prone to carbody or bogie hunting when the wheel-rail contact conicity is excessively low or high. This can cause negative impacts on vehicle dynamics performance. This study presents four types of typical yaw damper layouts for a high-speed locomotive (Bo-Bo) and compares, by using the multi-objective optimization method, the influences of those layouts on the lateral dynamics performance of the locomotive; the linear stability indexes under low-conicity and high-conicity conditions are selected as optimization objectives. Furthermore, the radial basis function-based high-dimensional model representation (RBF-HDMR) method is used to conduct a global sensitivity analysis (GSA) between key suspension parameters and the lateral dynamics performance of the locomotive, including the lateral ride comfort on straight tracks under the low-conicity condition, and also the operational safety on curved tracks. It is concluded that the layout of yaw dampers has a considerable impact on low-conicity stability and lateral ride comfort but has little influence on curving performance. There is also an important finding that only when the locomotive adopts the layout with opening outward, the difference in lateral ride comfort between the front and rear ends of the carbody can be eliminated by adjusting the lateral installation angle of the yaw dampers. Finally, force analysis and modal analysis methods are adopted to explain the influence mechanism of yaw damper layouts on the lateral stability and differences in lateral ride comfort between the front and rear ends of the carbody.

Key words: High-speed locomotive; Yaw damper layout; Lateral stability; Lateral ride comfort; Multi objective optimization; Global sensitivity analysis (GSA)

1 Introduction

The yaw damper, as one of the important suspension components of railway vehicles, is installed longitudinally between the bogie frame and the carbody. It can significantly attenuate the lateral vibration of the bogie frame and suppress the carbody's yaw motion, thus enhancing the critical speed of vehicles. Therefore, a reasonable selection of yaw damper parameters is particularly important to improve the lateral ride comfort of the carbody and to reduce the wheel-rail lateral force (Wang et al., 2011, 2014; Persson et al., 2014; Zhang et al., 2021). Yan and Zeng (2018) and Yan et al. (2019) analyzed the influence of the yaw damper's damping and series stiffness on the bogie stability and bifurcation type in detail. They combined the central popular theorem and the paradigm method to obtain expressions for critical speed and bifurcation types related to the damping and series stiffness of the yaw damper, and showed qualitatively the influence trend of the yaw damper's damping and series stiffness on the bifurcation type of bogies. Zeng et al. (2021) studied the stochastic failure process of damper elements and its influence on the dynamics performance of railway vehicles, and the results showed that the deterioration of failure probability and damping reduction amplitude would cause stronger vibrations. Among them, the stochastic failure of the secondary lateral damper and the yaw damper was harmful to lateral vehicle dynamics, which fully demonstrated the importance of yaw dampers on railway vehicles. Xia et al. (2020) constructed a bogie mechanical model with four degrees of freedom (DOFs) in

✉ Yuan YAO, yyuan8848@163.com
Guang LI, https://orcid.org/0000-0002-3190-0357
Yuan YAO, https://orcid.org/0000-0003-2279-7463

Received Aug. 11, 2022; Revision accepted Nov. 23, 2022; Crosschecked Mar. 7, 2023

which the constitutive relationship of yaw dampers was considered, and analyzed the influence of damper parameters and installation position on stability, comfort, and steering ability. It was found that the larger lateral installation position and damping, as well as relatively small stiffness, were beneficial to the bogie lateral stability, and the design trend based on stability and comfort was consistent but contradictory to the curving performance. Aiming at the low-frequency swaying phenomenon of the carbody for HEMU-430X, Jeon et al. (2016) found that, through simulation results and experimental data, the carbody hunting instability phenomenon disappeared after the position of yaw dampers was changed, and analyzed whether the position of yaw dampers could generate a yaw torque to explain the influence mechanism, from the perspective of a single bogie. This shows that the yaw damper layout also holds a notable effect on the lateral dynamics performance of railway vehicles. However, there are relatively few scholars studying the yaw damper layout.

Yaw damper parameters and layouts have different influences on multiple vehicle dynamics performance indexes, which belongs to the multi-objective problem. Multi-objective optimization is widely applied in multiple fields of railway vehicles and is a useful technique for resolving actual engineering challenges, where the genetic algorithm (GA) is frequently utilized because it demonstrates notable superiority over the majority of intelligent search algorithms, including the highest likelihood of global optimization (Goldberg, 1989). Johnsson et al. (2012) conducted the optimization of damping characteristics in bogie suspensions employing the GA, with the aim of enhancing the ride comfort and running safety for railway vehicles. Mousavi-Bideleh and Berbyuk (2016a, 2016b) and Mousavi-Bideleh et al. (2016) adopted GAs to perform the wear/comfort Pareto optimization of some bogie suspension components, which is for a railway vehicle dynamics model owing 50 DOFs. Jiang et al. (2020) employed GAs to optimize the curving dynamics performance of articulated monorail vehicles and pointed out that the multi-parameter and multi-objective optimization method could be used for other types of railway vehicles. Pålsson and Nielsen (2012) presented to optimize the specified track gauge variation in the switch panel of railway turnouts to reduce track profile wear through a GA, and two different vehicle models of freight car and passenger car were established, where research results showed that the optimal gauge configuration was uniform for both vehicle types. Besides, Yao et al. (2020) and Chen et al. (2022) proposed the concept of robust of hunting stability for high-speed trains, and the improved non-dominated sorting genetic algorithm NSGA-II was utilized to optimize suspension parameters, obtaining the suspension parameters matching law for high-speed trains. Li et al. (2022) carried out the multi-objective optimization of several suspension parameters with respect to lateral stability and ride comfort for the high-speed locomotive (Bo-Bo) by GAs, and extracted the matching relationship of suspension parameters through data analysis methods. Three types of combination modes of suspension parameters were proposed, and it was pointed out that there is a strong positive correlation between lateral ride comfort and stability under the low-conicity condition.

The yaw damper parameters and layouts are closely related to the carbody lateral ride comfort. In recent years, Chinese high-speed locomotives with a speed of v=200 km/h have appeared the phenomenon of carbody hunting when running on some special sections of straight track, seriously affecting the ride comfort of passengers and drivers. This phenomenon has attracted extensive attention from locomotive and vehicle manufacturers and researchers. Studies have shown that the carbody hunting instability caused by low wheel-rail contact conicity is an important reason for the low-frequency swaying phenomenon, and some solutions, such as adjusting the suspension parameter and re-profiling the rail profile, have been proposed (Sun et al., 2021). Thus, the intention of this study is to research the effect of yaw damper layouts on the lateral dynamics performance of locomotives, including lateral stability, ride comfort, and curving performance.

2 Multibody modelling

The composition of the locomotive dynamics model with 90 DOFs is presented in this section, which is developed in SIMPACK software, and four typical layouts of yaw dampers are described. Besides, track conditions and irregularities, as well as the MATLAB/SIMPACK co-simulation platform adopted in the following simulations, are introduced.

2.1 High-speed locomotive dynamics model

A high-speed locomotive (Bo-Bo) dynamics model with 90 DOFs is developed in SIMPACK software (Fig. 1). The model contains one carbody, two bogie frames, four wheelsets, two traction rods, four motors, and four hollow shafts as well as eight rotary arm bodies, a total of 25 rigid bodies (Tao et al., 2021; Shao et al., 2022). There are six DOFs in space for some bodies, which include the carbody, bogie frames, and wheelsets as well as motors. Every hollow shaft allows lateral, rolling, and yaw motions around the wheelset, each traction rod owns two DOFs including yaw and pitch motions for the carbody, and every rotary arm only holds a rotation motion for the wheel axle. The wheel/rail functions are built based on the CN60 rail and JM3 wheel profiles (Lyratzakis et al., 2021), and the track gauge is set to 1.435 m. The FASTSIM algorithm is adopted to compute the creep force (Kalker, 1982), where the Kalker weighting factor is 1, and the algorithm is based on Kalker's simplified theory, in which the wheel-rail contact model belongs to Hertz type. The main dynamics parameters for the model are shown in Table S1 of the electronic supplementary materials (ESM).

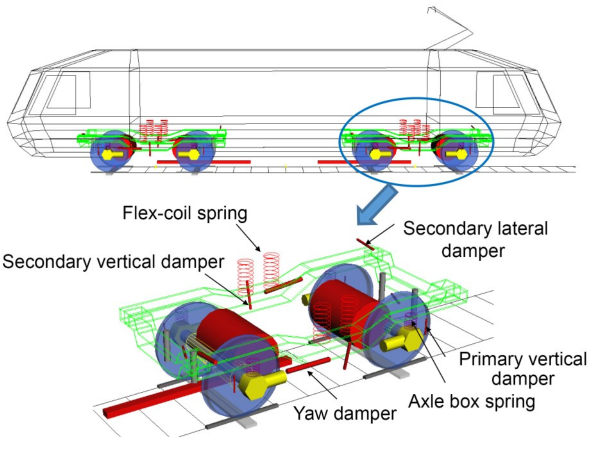

Fig. 1 High-speed locomotive dynamics model

The bogie suspension system consists of many suspension elements, which can be divided into two major categories: primary suspension and secondary suspension. Specifically, the primary suspension acts between the wheelset and bogie frame, which includes rotary arms, axle box springs, and primary vertical dampers. The secondary suspension works between the bogie frame and carbody, involving the secondary lateral damper, secondary vertical damper, yaw damper as well as flex-coil spring, and secondary lateral stoppers are also established. Moreover, the locomotive model considers the nonlinear characteristics of all dampers and stop elements in the form of a piecewise function and all the dampers are modeled using the Maxwell model. Besides, the Wuhan–Guangzhou high-speed rail track spectrum (Li et al., 2014) is used for the following time-domain simulations on straight and curved tracks. It should be noted that the accuracy of the locomotive dynamics model has been verified through on-track test results described in a previous study (Li et al., 2022).

2.2 Yaw damper layouts

According to practical engineering experience, four types of yaw damper layouts are proposed, whose schematic diagrams are shown in Fig. 2. The layouts are named by reference to their opening form and the connection positions of the yaw dampers on the bogie frame and carbody. Comparing Figs. 2a and 2b, we can conclude that the layout form of yaw dampers on both sides of a single bogie is symmetrical about the longitudinal centerline of the bogie frame. The opening direction of the former is towards the carbody center, but the opening direction of the latter is away from the carbody center, so they are named as opening inward (OI) and opening outward (OO), respectively. In Figs. 2c and 2d, it can be seen that yaw dampers on both sides of a single bogie are arranged symmetrically with respect to the center of bogie frame. The connection position of yaw dampers on the bogie frame is close to the horizontal centerline of bogie frame for the former, but the connection position on the carbody is adjacent to the horizontal centerline for the latter. Therefore, the last two layouts

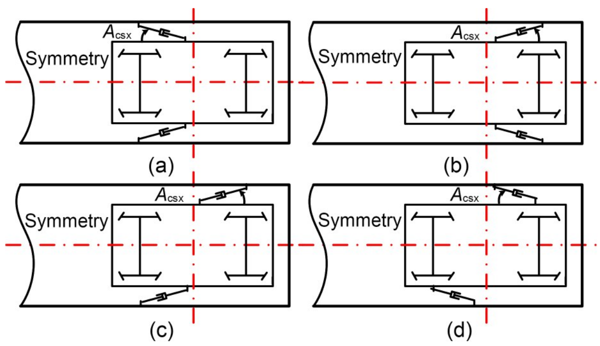

Fig. 2 Schematic diagram of yaw damper layouts: (a) OI; (b) OO; (c) SS; (d) ASS

are called skew symmetry (SS) and anti-skew symmetry (ASS). The yaw damper damping C_{sx} and its series stiffness K_{ncsx} as well as lateral installation angle A_{csx} are all considered in the research.

2.3 MATLAB/SIMPACK co-simulation platform

During the multi-objective optimization and Monte Carlo simulations for vehicle dynamics performance, the optimization algorithms or sampling methods are generally completed in MATLAB, but the modelling and calculation for the locomotive dynamics model are implemented by SIMPACK. Consequently, it is extremely critical to connect MATLAB and SIMPACK software to accomplish the optimization and simulation procedures. Here, the MATLAB/SIMPACK co-simulation platform is established via SIMPACK script languages, including the pre-processing language ‘sjs’ and post-processing language ‘qs’, which are specific coding languages of SIMPACK. Concretely, the function of ‘sjs’ language is to modify values of optimized parameters and perform simulation calculations, and the action of ‘qs’ language is to obtain simulation results. Fig. 3 is the specific flowchart of the MATLAB/SIMPACK co-simulation platform, where a sequence of ‘sjs’ and ‘qs’ languages can be edited and executed by MATLAB, and the co-simulation process will be terminated when the prescribed maximum iteration number or sample times are reached. Finally, optimization results can be saved in MATLAB, and data analysis, such as a sensitivity analysis, can also be conducted.

3 Dynamics evaluation index

This section presents the definition, calculation, and evaluation methods of lateral stability, lateral ride comfort, and operation safety indexes, which all refer to the GB/T 5599-2019 standard (SAMR, 2019), and the above evaluation indexes will be used in the following Pareto optimization and analysis of suspension parameters.

3.1 Lateral stability

Lateral stability is one of the most basic dynamics requirements for railway vehicles, and ensures that the vehicles can run on tracks stably. Generally, the lateral stability of railway vehicles system includes linear stability and nonlinear stability. The former is adopted to evaluate lateral stability of the studied locomotive, which can considerably reduce the computational workload and meanwhile describe the lateral stability to some extent (Polach, 2006a, 2006b). The linear stability is calculated for the linearized locomotive dynamics model, whose essence is to solve eigenvalues and eigenvectors of the Jacobian matrix for the vehicle linear system. The calculation equations are as follows:

$$\eta = a + b\mathrm{i}, \tag{1}$$

$$f = |b|/(2\pi), \tag{2}$$

$$\zeta = a\Big/\sqrt{a^2+b^2}\,. \tag{3}$$

In Eq. (1), i represents the imaginary unit and η indicates the eigenvalue of the linear system; the symbols a and b stand for the corresponding real part and imaginary part, respectively. As Eq. (2) shows, f represents the modal vibration frequency, which can reflect the vibration level of the system. In Eq. (3), the symbol ζ stands for the modal vibration-damping ratio, defined as the linear stability index; the system is considered stable if the value of ζ is smaller than zero. Also, the

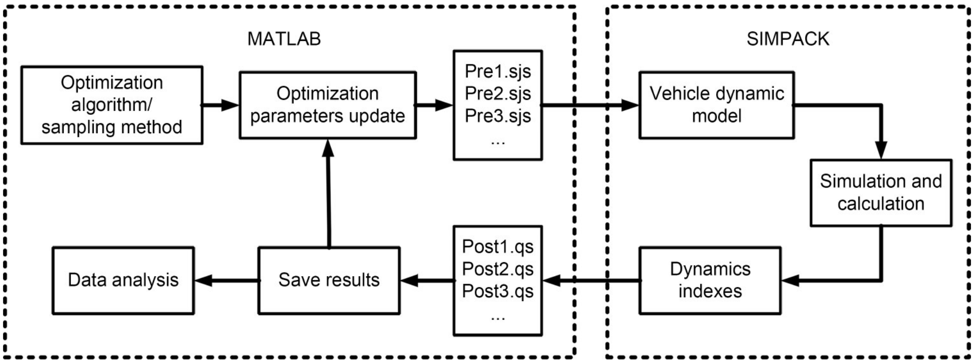

Fig. 3 Flowchart of the MATLAB/SIMPACK co-simulation platform

vehicle system is regarded to be stable enough when the index ζ is smaller than −0.05 (Polach, 2006a).

3.2 Lateral ride comfort

Many developed railway countries have individual evaluation systems for ride comfort, such as the Chinese GB/T 5599 (SAMR, 2019), European UIC 513 (IUR, 1994), and international standard ISO 2631 (ERRI, 1989), which are mostly used to evaluate the comfort of passengers or drivers on trains and the integrity of goods loaded on railway trucks. The ride comfort index is formulated for evaluating the carbody's random vibration. The Sperling index is usually used to appraise the ride comfort for railway vehicles. It contains the lateral and vertical ride comfort indexes, and the former is the one examined here. The calculation equation of the lateral ride comfort index W_{y} is expressed as (SAMR, 2019):

$$W_{\mathrm{y}}=3.57\sqrt[10]{\frac{A_{\mathrm{y}}^{3}}{f_{\mathrm{a}}}F(f_{\mathrm{a}})}. \tag{4}$$

As Eq. (4) shows, A_{y} represents the lateral acceleration amplitude in the frequency domain, f_{a} indicates the corresponding frequency, and $F(f_{\mathrm{a}})$ stands for the frequency correction coefficient. In the calculation procedure of W_{y}, the measurement location is generally the carbody floor. To study the difference in lateral ride comfort between the front and rear ends of the carbody, lateral accelerations at the carbody's front and rear ends are both extracted, and the corresponding lateral ride comfort indexes are obtained, which are represented by W_{yf} and W_{yr}, respectively. The limit value for an excellent level of locomotive lateral ride comfort is 2.75, and smaller values of W_{y} represent a better lateral ride comfort performance.

3.3 Operational safety

Generally, the operational safety constraints for railway vehicles are very extensive, including the vehicle dynamics performance and structural strength as well as track response. However, only evaluation indexes for operational safety related to the vehicle lateral dynamics performance are studied here. The operational safety indexes are often related to the force of railway vehicles on tracks, such as the wheelset lateral force, derailment coefficient, and overturning coefficient. These indexes are relatively large when railway vehicles run on curved tracks, and the overturning coefficient is primarily utilized to evaluate the operational safety of a vehicle running under crosswind conditions. Thus, in this study, the wheelset lateral force $\mathit{\Gamma}_{\mathrm{WF}}$ and derailment coefficient $\mathit{\Gamma}_{\mathrm{DC}}$ are selected to evaluate the locomotive's curving dynamics performance.

The wheelset lateral force $\mathit{\Gamma}_{\mathrm{WF}}$ is the algebraic sum of the left and right wheel-rail lateral forces on the same wheelset and evaluates whether the track gauge will be widened or tracks will be severely deformed because of the excessive lateral force during vehicle operation. In addition, there are various dynamics standards concerning the evaluation value of the wheelset lateral force. The calculation equation of the adopted evaluation method is as follows:

$$\mathit{\Gamma}_{\mathrm{WF}}\leqslant 15+P_{0}/3, \tag{5}$$

where P_0 is the static axle weight, and the limit value of $\mathit{\Gamma}_{\mathrm{WF}}$ is about 78 kN for the locomotive studied here.

The derailment coefficient $\mathit{\Gamma}_{\mathrm{DC}}$ is formulated according to the derailment condition of wheel climbing, and is used to assess whether the wheel rim of a railway vehicle will climb onto the rail head and even derail under the action of lateral forces. The calculation method and critical value calculation equations are defined as:

$$\mathit{\Gamma}_{\mathrm{DC}}=Y/Q=\frac{\tan\alpha-\mu}{1+\mu\tan\alpha}. \tag{6}$$

In Eq. (6), Y and Q are the lateral force and vertical force, respectively, acting on the rail by the wheels on the climbing rail side, and α and μ are the wheel flange angle and wheel-rail friction coefficient, respectively. In the practical calculation of the derailment coefficient, it is only required to extract values of Y and Q, and $\mathit{\Gamma}_{\mathrm{RD}}$ is the ratio of Y to Q on the same wheelset. Besides, when the curve radius of operation conditions is within the range of 250–400 m, the limited value of $\mathit{\Gamma}_{\mathrm{DC}}$ is 0.9, and a smaller value of $\mathit{\Gamma}_{\mathrm{RD}}$ means that the railway vehicle has a better operational safety performance.

4 Multi-objective optimization

In this section, several low-conicity/high-conicity stability Pareto optimization problems are formulated and solved for locomotive models with four layouts of yaw dampers and the matching relationship between yaw damper layouts and suspension parameters for the locomotive's lateral stability is determined.

4.1 Optimization scenarios

Lateral stability is one of the most important dynamics performances for railway vehicles. The primary function of yaw dampers is to improve lateral stability for the vehicle system. Moreover, lateral stabilities under low-conicity and high-conicity conditions are generally contradictory and must be simultaneously satisfied in the design of railway vehicles. The purpose of this study is to analyze the influence of yaw damper layouts on the locomotive's lateral dynamics performance. Since an excessive number of optimization objectives is harmful when comparing the influence results, only the low-conicity stability index ζ_{low} and high-conicity stability index ζ_{high} are selected as optimization objectives and for which equivalent conicities at 3 mm of wheel-rail relative displacement are 0.04 and 0.40, respectively. The detailed settings for the two objectives are shown in Table 1.

Table 1 Optimization indexes and operation settings

Index	Calculation condition		Wheel tread	Rail cant
	v (km/h)	Conicity		
ζ_{low}	200	0.04	JM3_new	1/20
ζ_{high}	200	0.40	JM3_wear	1/40

The optimization direction is to obtain smaller values of both optimization objectives simultaneously, and Γ stands for the objective functions, as shown in Eq. (7).

$$\Gamma = \min\left\{\zeta_{low}, \zeta_{high}\right\}. \tag{7}$$

In the low-conicity/high-conicity stability Pareto optimization, the design parameters contain the yaw damper's damping, series stiffness, and lateral installation angle in the horizontal plane, which are closely related parameters of the yaw damper. Among the above three parameters, the lateral installation angle A_{csx} can reflect the yaw damper layout to a certain extent, which means that we can judge the influence of yaw damper layouts on the locomotive's dynamics performance by observing the variation of A_{csx}. In addition, the primary longitudinal stiffness and lateral stiffness as well as the secondary lateral damper damping are also considered. The optimization ranges of the design parameters are shown in Table 2.

Table 2 Design parameters and optimization ranges

Parameter	Design range
Damping of yaw damper, C_{sx} (kN·s/m)	200–2000
Series stiffness of yaw damper, K_{ncsx} (kN/mm)	10–50
Lateral installation angle of yaw damper, A_{csx} (°)	0–10
Primary longitudinal stiffness, K_{px} (kN/mm)	10–100
Primary lateral stiffness, K_{py} (kN/mm)	2–10
Damping of secondary lateral damper, C_{sy} (kN·s/m)	10–60

In addition, the genetic algorithm NSGA-II has been used for the low-conicity/high-conicity stability Pareto optimization, which is conducted based on the MATLAB/SIMPACK co-simulation platform. The values of population size and generation number are 5000 and 12, respectively. Also, the crossover probability is set to 0.8 and the mutation probability is set to 0.2.

4.2 Optimization results

To fully research the influence of yaw damper layouts on lateral stability, two optimization levels are carried out for the locomotives under four types of yaw damper layouts. Specifically, in the first optimization level, the lateral installation angle A_{csx} is a fixed value of 4°, which means that the value of A_{csx} is not involved in the optimization, but A_{csx} is optimized in the second optimization level. The low-conicity/high-conicity stability objective functions (Pareto fronts) for the two optimization levels are shown in Fig. 4, where the hollow and solid dots represent Pareto fronts for the first and second optimization levels, respectively, and Figs. 4a–4d correspond to the four layouts: OI, OO, SS, and ASS.

In Fig. 4, the horizontal and vertical axes represent low-conicity stability and high-conicity stability indexes, respectively. A_{csx}=4° stands for that A_{csx} is a fixed value, and A_{csx} opt represents that A_{csx} is optimized. It can be concluded that, for the OI or OO layout, the optimal low-conicity stability has been improved when A_{csx} is involved in the optimization. However, when the SS or ASS layout is selected by the locomotive, the Pareto fronts for the two optimization levels are consistent, which shows the value of A_{csx} has almost no effect on the lateral stability. In addition, it can be learnt that, no matter which type of yaw damper layout is adopted, the low-conicity and high-conicity stabilities of the locomotive can always meet practical operating requirements through Pareto optimization.

Fig. 5 shows the optimized values of suspension parameters (Pareto sets) for the second optimization level, and the four symbols represent the four layouts of yaw dampers respectively. The horizontal axis indicates the low-conicity stability index ζ_{low}, and the vertical axis of each subgraph represents the suspension parameter. It can be seen that no matter which type of yaw damper layouts is used, the distribution trend of C_{sx}, K_{ncsx}, K_{px}, and K_{py} to the low-conicity stability is consistent. Specifically, smaller values of C_{sx}, K_{ncsx}, and K_{px} are conducive to low-conicity stability, but the value of K_{py} has little effect on the locomotive's lateral stability. Besides, when the OI layout is adopted, the values of C_{sy} are concentrated in the range of 55–60 kN·s/m, which implies that a larger value of C_{sy} is demanded for the locomotive. In addition, there is an interesting phenomenon that the distribution of A_{csx} shows some notable distinctions when the locomotive adopts the four layouts of yaw dampers. Specifically, for the OI layout, the value of A_{csx} is concentrated at 0°–3°, which means that a smaller value of A_{csx} is required. When the locomotive adopts the OO layout, the value of A_{csx} is distributed in the range of 5°–10°. For the SS or ASS layout, the value of A_{csx} is evenly distributed in the range of 0°–10°. The above conclusions may reflect that there are significant matching relationships between the yaw damper layout and the value of A_{csx}, and prove that the layouts can affect the low-conicity stability. The low conicity stability is usually closely related to the carbody lateral ride comfort, so

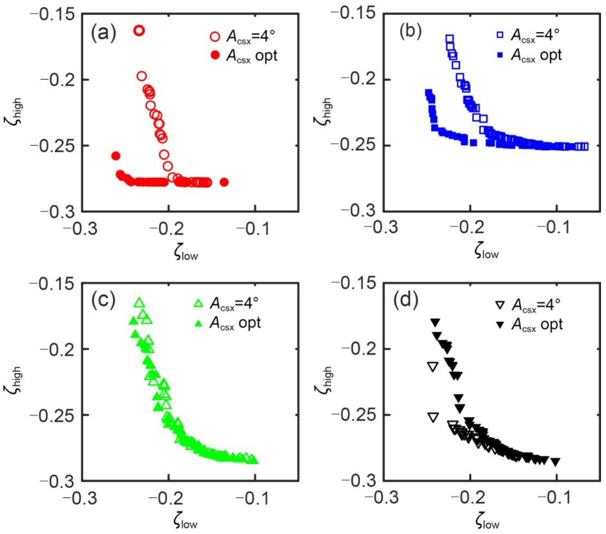

Fig. 4 Pareto fronts for locomotive under four yaw damper layouts: (a) OI; (b) OO; (c) SS; (d) ASS

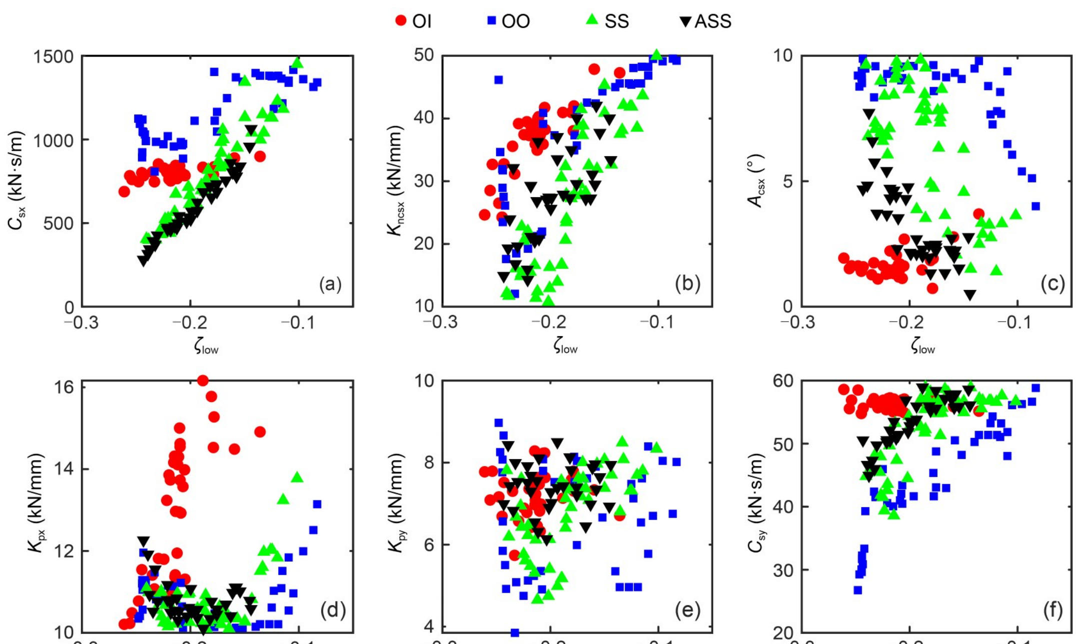

Fig. 5 Distributions of Pareto sets regarding ζ_{low}: (a) C_{sx}; (b) K_{ncsx}; (c) A_{csx}; (d) K_{px}; (e) K_{py}; (f) C_{sy}

the effect of yaw damper layouts on lateral ride comfort under the low-conicity condition is investigated in the next subsection.

5 Parameter analysis methods and results

This section introduces the data analysis method of global sensitivity analysis (GSA) and the sampling method. It deals with time-domain simulations when the locomotive runs in two operational scenarios including straight track under the low-conicity condition and curved track. Then, the influences of yaw damper layouts and suspension parameters on lateral ride comfort on the straight track and curving performance are investigated.

5.1 GSA method

GSA can provide a good understanding for evaluating the importance of design parameters and decreasing the number of design parameters, so as to reduce the computational burden. Nevertheless, the locomotive dynamics model has complex structures and nonlinear suspension elements, which would significantly affect the precision of GSA, so the surrogate model method may provide an effective solution to the problem. Traditional surrogate models principally include the response surface, neural network, and Kriging surrogate model (Ye et al., 2020), which can handle low-dimensional problems well, but large errors may occur when dealing with nonlinear complex systems. However, high-dimensional model representation (HDMR) can successfully solve the problems (Simpson et al., 2004; Tunga and Demiralp, 2005; Shao and Wang, 2010), and thus it is used to conduct the GSA between the locomotive's lateral dynamics performance and the key suspension parameters.

There are various extended forms of HDMR, but the Cut-HDMR requires only simple arithmetical calculations and provides the lowest cost model with an accuracy comparable to other HDMR types. It is widely used to tackle engineering problems with low coupling characteristics, but the Cut-HDMR lacks incidental sampling methods and cannot present a complete model. However, the radial basis function (RBF)-HDMR can make up for the above drawbacks of Cut-HDMR, where the RBF is integrated into the component of Cut-HDMR to construct the RBF-HDMR model.

The RBF model is generally expressed as:

$$f(x)=\sum_{i=1}^{h} w_i\phi(\|x-\boldsymbol{u}_i\|)+b_0, \tag{8}$$

where x and $f(x)$ represent the input and output terms, respectively; h is the number of RBF hidden layer neurons; $\boldsymbol{u}_i$ indicates the center vector of the hidden layer nodes. Also, b_0 is the bias value, and w_i stands for the weight. The symbol '$\|\cdot\|$' represents the Euclidean norm, and $\phi(\cdot)$ indicates the Gaussian RBF.

Cut-HDMR is defined as:

$$f(x)=f_0+\sum_{i=1}^{m} f_i(x_i)+\sum_{1\leqslant i<j\leqslant m} f_{ij}(x_i, x_j). \tag{9}$$

In Eq. (9), f_0 is a constant term, $f_i(x_i)$ represents the effect of the variable x_i on the response function when x_i alters alone, $f_{ij}(x_i, x_j)$ stands for coupling effects between x_i and x_j, and m is the number of input parameters.

Hence, RBF-HDMR based on Cut-HDMR is expressed as follows:

$$\hat{f}(x)=f_0+\sum_{i=1}^{M} \hat{f}_i(x_i)+\sum_{1\le i<j\le M} \hat{f}_{ij}(x_i, x_j), \tag{10}$$

where the symbol ^ represents the RBF model, and M indicates the number of samples.

GSA methods mostly include regression analysis, Fourier amplitude analysis, and variance-based analysis (Bigoni et al., 2014; Xu et al., 2018); the GSA method of variance-based analysis is adopted here.

$$S_i=\frac{D_i}{D}, \tag{11}$$

$$S_{ij}=\frac{D_{ij}}{D}, \tag{12}$$

where S_i stands for the independent impact of the variable x_i on outputs, and S_{ij} indicates the effect of parameter interactions between x_i and x_j. D represents the total variance, D_i stands for the total variance of $f_i(x_i)$, and D_{ij} indicates the partial variance of $f_{ij}(x_i, x_j)$. Therefore, the GSA index TS_i can be calculated as follows:

$$\mathrm{TS}_i=S_i+\sum_{j=1}^{M} S_{ij}. \tag{13}$$

5.2 Sampling method and Monte Carlo simulation

In this study we conduct GSA between the key suspension parameters and lateral dynamics performance of the locomotive from the perspective of time-domain simulations, where the analysis data is obtained through the Monte Carlo simulation and some procedures should be adopted to produce stochastic samples for suspension parameters. The simplest procedure is the standard Monte Carlo random sampling (SMCRS) method, which is generally based on the law of large numbers and requires plenty of samples to ensure the convergence speed. However, the time-domain simulation in SIMPACK software requires long computation times, so the Latin hypercube sampling (LHS) method is selected here. It can fully guarantee the uniformity of the sample space projection and decrease the sampling number required in the SMCRS method (Kassa and Nielsen, 2008; Shojaeefard et al., 2017).

The sampling number of LHS is set to 200, and the above six key suspension parameters are chosen as design parameters, whose sampling ranges are shown in Table 2. Then, the Monte Carlo simulation for time-domain simulations is carried out through the MATLAB/SIMPACK co-simulation platform, where straight and curved tracks are both considered, and the detailed settings about the tracks are shown in Table 3. Because the yaw damper layout has significant impact on the low-conicity stability, the lateral ride comfort indexes of the carbody's front and rear ends are both extracted for straight tracks under the low-conicity condition, and are represented by W_{yf} and W_{yr}, respectively. The maximum wheelset force Γ_{WF} and maximum derailment coefficient Γ_{DC} are drawn for curved tracks to evaluate the operational safety performance.

5.3 Parameters analysis results

The GSA results are shown in Fig. 6, and Figs. 6a–6d correspond to the analysis results between dynamics indexes W_{yf}, W_{yr}, Γ_{WF}, and Γ_{DC} to the suspension parameters. The horizontal axis represents the four layouts of yaw dampers, and the vertical axis stands for the global sensitivity coefficient TS, where a larger value of TS indicates that the corresponding sensitivity is stronger.

The GSA results show that W_{yf} and W_{yr} are sensitive to C_{sx} and A_{csx}, and the value of A_{csx} is more sensitive for the locomotive with OI or OO layout, as depicted in Figs. 6a and 6b. It can be concluded that yaw damper layouts have a significant effect on the locomotive lateral ride comfort on a straight track under the low-conicity condition. As Figs. 6c and 6d show, Γ_{WF} and Γ_{DC} are the most sensitive to C_{sx} and K_{py}, especially for the former, no matter which type of yaw damper layouts is adopted for the locomotive. However, Γ_{WF} and Γ_{DC} are not sensitive to A_{csx}, which implies that A_{csx} or even the layouts have little effect on the locomotive's curving performance.

In order to further study the influence of yaw damper layout on the carbody lateral ride comfort, when the locomotive runs on straight track under the low-conicity condition, the calculated results of W_{yf} and W_{yr} with the variation of A_{csx} are shown in Table 4. There is an interesting phenomenon that A_{csx} has a negative correlation with W_{yr} only for the locomotive with OO layout, which indicates that a larger value of A_{csx} can help to improve the lateral ride comfort of the carbody's rear end. In addition, when the value of A_{csx} is zero, the value of W_{yr} is always greater than W_{yf}. Therefore, an appropriate value of A_{csx} can reduce or even eliminate the difference in lateral ride comfort between the front and rear ends of the carbody, which is the unique characteristic of the OO layout for the locomotive compared with the other three layouts.

6 Discussion

This section deals with the mechanism analysis for the matching relationship between yaw damper layouts and lateral installation angle A_{csx}; the influence of the layouts on the difference in lateral ride comfort between the carbody's front and rear ends is also explained, where the force analysis and modal analysis methods are adopted for the whole carbody.

Table 3 Detailed settings of the tracks for Monte Carlo simulation

Track	Radius (m)	Superelevation (mm)	v (km/h)	Index	Rail cant	Condition
Straight	∞	–	200	W_{yf}, W_{yr}	1/20	Low-conicity
Curved	300	125	70	Γ_{WF}, Γ_{DC}	1/40	Normal-conicity

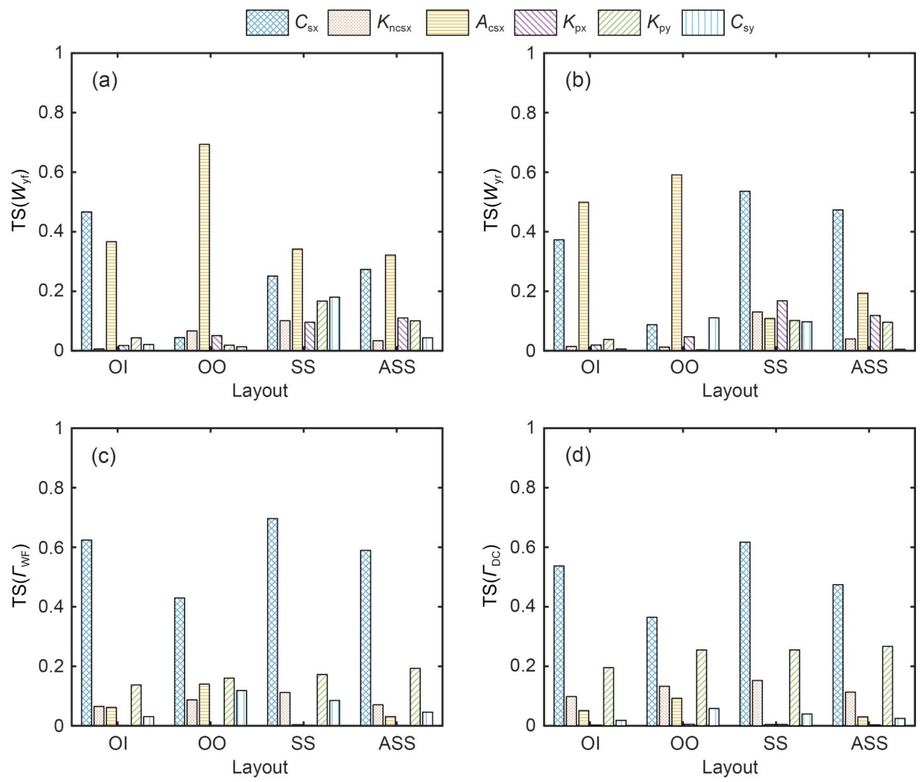

Fig. 6 GSA results between dynamics indexes W_{yf} (a), W_{yr} (b), Γ_{WF} (c), and Γ_{DC} (d)

Table 4 Calculated results of W_{yf} and W_{yr} with the variation of A_{csx}

A_{csx} (°)	OI		OO		SS		ASS	
	W_{yf}	W_{yr}	W_{yf}	W_{yr}	W_{yf}	W_{yr}	W_{yf}	W_{yr}
0	2.14	2.61	2.15	2.64	2.15	2.64	2.14	2.61
2	2.09	2.61	2.19	2.61	2.15	2.62	2.18	2.65
4	2.13	2.65	2.20	2.52	2.16	2.61	2.23	2.69
6	2.24	2.76	2.23	2.42	2.18	2.61	2.28	2.72
8	2.37	3.00	2.27	2.32	2.22	2.61	2.33	2.76
10	2.39	3.00	2.34	2.23	2.26	2.62	2.38	2.80

6.1 Force analysis

Since the yaw damper layout of the front/rear bogie under the OI layout is the same as that of the rear/front bogie under the OO layout, it is unreasonable to carry out the mechanism analysis for the single bogie, and, in this study, the mechanism analysis for matching relationships between the layouts and A_{csx} is aimed at the whole carbody. For railway vehicles running on straight tracks, when the value of A_{csx} is unequal to zero and there exists a lateral motion between the carbody and bogie frame, the length of the yaw dampers will change, which could result in additional displacement and velocity at both ends of the yaw damper, generating an additional force F' between the carbody and bogie frame. The calculation formula of F' is as follows:

$$F' = K_e \cdot \Delta y \cdot \sin A_{csx} + C_e \cdot \Delta\dot{y} \cdot \sin A_{csx}. \qquad (14)$$

In Eq. (14), Δy and $\Delta\dot{y}$ represent the relative lateral displacement and velocity at both ends of the yaw damper, respectively, and K_e and C_e stand for the equivalent lateral stiffness and damping of the yaw dampers, respectively. It can be concluded that the additional force F' is related to the value of A_{csx}, and that F' would increase with the increase of A_{csx}. Moreover, there is no additional force for the above yaw damper layouts when the value of A_{csx} is zero, and the original value of A_{csx} is 4° for the locomotive. When the value of Δy is 20 mm, the additional displacement of the yaw damper is about 1.4 mm, which is close to half of the action stroke of the yaw damper. Consequently, the value of F' is about half of the yaw damper's output force, and its impact on the locomotive's dynamics performance cannot be ignored.

Because the force analysis of the OI/ASS is similar to that for the OO/SS layout, the force analysis regarding the OO and SS layouts is taken as an example for explanation. Assuming that the bogie frame is fixed, when the carbody occurs a lateral or yaw motion, the action direction and effect of the additional force F' and the additional torque T_c', which are generated by yaw dampers on the carbody are analyzed, and schematic diagrams of that force analysis are shown in Fig. 7. In the figure, the additional force exerted on the carbody by each yaw damper is represented by F_{11}', F_{12}', F_{21}', and F_{22}', and the additional torques applied to the front and rear ends of the carbody are expressed by T_{cf}' and T_{cr}'. In addition, the action direction of F' is along the layout direction of the yaw dampers, and the generation of T_{cf}' and T_{cr}' that is studied considers only the longitudinal component of F', because the lateral component of F' is minor and its impact on lateral dynamics performance is negligible.

As Figs. 7a and 7b depict, when the carbody only has a lateral motion y_c, the lateral component of F' always prevents the carbody's lateral movement. For the OO layout, the directions of T_{cf}' and T_{cr}' are opposite, so the combined additional torque T_c' to the carbody center is minor. However, when the SS layout is adopted by the locomotive, the values of T_{cf}' and T_{cr}' are both equal to zero, which naturally implies that no additional torque is applied on the carbody. The above conclusions reveal that when the carbody only has lateral motion, the combined additional torques T_c' are all small for the locomotive with the two layouts.

In Figs. 7c and 7d, when the carbody incurs only a yaw motion φ_c, the front and rear ends of the carbody will produce opposite lateral motions, which are represented by y_{cf}' and y_{cr}'. For the OO layout, the action directions of T_{cf}' and T_{cr}' are the same as the direction of the carbody' yaw motion, which is equivalent to reducing the rotation stiffness or damping to resist the yaw motion. For the low-conicity stability, it is necessary to reduce the rotational coupling between the carbody and bogie frame. A larger value of A_{csx} is beneficial to reducing the coupling effect of the carbody and bogie frame, but the excessive angle will further weaken the coupling effect, which is also harmful to the locomotive's lateral stability. Therefore, a moderate value of A_{csx} should be provided to suit the locomotive with OO layout, which can improve the low-conicity stability. For the SS layout, the values of T_{cf}' and T_{cr}' are both equal to zero, so the value of A_{csx} has little effect on the locomotive's lateral stability.

6.2 Modal analysis

To research the influence mechanism of yaw damper layouts on the difference in lateral ride comfort between the front and rear ends of the carbody, the modal analysis is conducted for the high-speed locomotive dynamics model. Generally, the speed root locus is very common and used to search the linear critical speed of railway vehicles, but the root locus

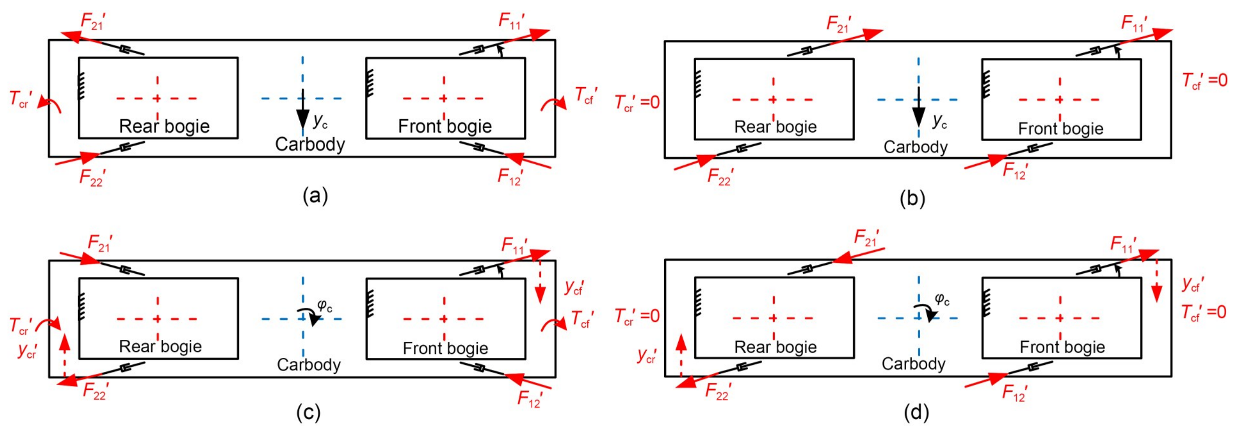

Fig. 7 Schematic diagrams of force analysis of the carbody incurring a lateral or yaw motion: (a) lateral motion, OO; (b) lateral motion, SS; (c) yaw motion, OO; (d) yaw motion, SS

that varies with the lateral installation angle A_{csx} is utilized here, and the phase lag between the carbody's lateral and yaw motions corresponding to the hunting modal is obtained.

The calculated root locus curves with the variation of A_{csx} are shown in Fig. 8, and the low-conicity condition is only considered here because the high-conicity stability is generally better and hardly affected by the lateral installation angle A_{csx}. In the figure, the abscissa axis represents the modal damping ratio ζ, and the ordinate axis indicates the modal frequency f. Besides, Figs. 8a–8d correspond to the locomotive under the four layouts of yaw dampers, and every root locus is composed of 11 groups of characteristic roots with the value of A_{csx} range of 0°–10°, where each 'circle' indicates a corresponding modal under a certain value of A_{csx}. Also, the larger the circle symbol implies that the corresponding yaw damper layout adopts a larger value of A_{csx}. It can be concluded that when the locomotive adopts the OI layout, decreasing the value of A_{csx} is favorable for the locomotive's lateral stability. When the locomotive employs the OO layout, a moderate value of A_{csx} is beneficial to the lateral stability, and there exists an optimal value of A_{csx}. However, the value of A_{csx} has little effect on the lateral stability when the SS or ASS layout is utilized by the locomotive.

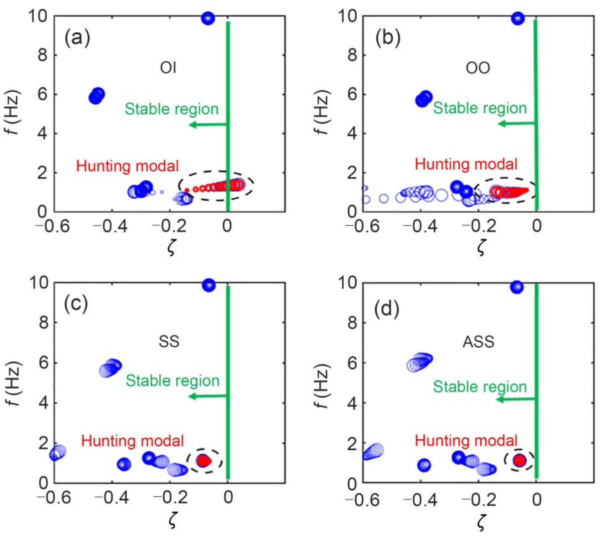

Fig. 8 Root locus curves with the variation of A_{csx}: (a) OI; (b) OO; (c) SS; (d) ASS

The phases of the carbody's lateral and yaw motions corresponding to the hunting modal are extracted from Fig. 8, and the phase lag between the lateral and yaw motions is calculated, with results shown in Fig. 9. The horizontal axis represents the value of A_{csx}, and the vertical axis indicates the phase lag between the carbody's lateral and yaw motions. It can be found that when the value of A_{csx} is equal to zero, the phase lags are almost the same for locomotives with the four layouts. For the OI layout, the phase lag would be enlarged with the increase of A_{csx}, but the value of A_{csx} has little influence on the phase lag when the SS or ASS layout is adopted by the locomotive. Only when the OO layout is employed, a larger value of A_{csx} can decrease the phase lag, and the difference in lateral ride comfort between the front and rear ends of the carbody can be reduced or even eliminated, so the OO layout for the locomotive is better than other three layouts from this point of view.

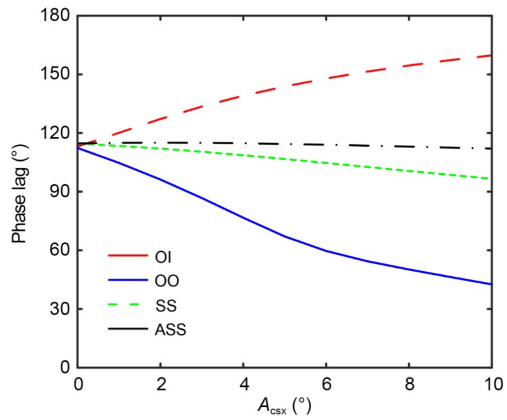

Fig. 9 Phase lag results between the carbody's lateral and yaw motions

When the carbody's lateral motion $\boldsymbol{y}_c$ and yaw motion $\boldsymbol{\varphi}_c$ occur simultaneously, the lateral movements of the front and rear ends of the carbody are expressed as follows (Alfi et al., 2008; Yao et al., 2015):

$$\begin{cases} \boldsymbol{y}_{cf} = \boldsymbol{y}_c + \boldsymbol{\varphi}_c \cdot l, \\ \boldsymbol{y}_{cr} = \boldsymbol{y}_c - \boldsymbol{\varphi}_c \cdot l. \end{cases} \tag{15}$$

In Eq. (15), $\boldsymbol{y}_{cf}$ represents the lateral movement of the carbody's front end, $\boldsymbol{y}_{cr}$ stands for the lateral movement of the carbody's rear end, and l is half of the longitudinal distance between the front and rear ends of the carbody.

Ideally, there should exist a 90° phase lag between lateral and yaw motions of the carbody so the lateral ride comfort of the carbody's front and rear ends is consistent. In reality, the phase lag between the lateral and yaw motions corresponding to the hunting modal is greater than 90°, especially when the equivalent conicity of wheel-rail contact is low, as shown in Fig. 9. Besides, the lateral additional force $\boldsymbol{F}_y'$ and torque $\boldsymbol{T}_y'$ produced by the yaw damper are related to the magnitude of the lateral displacement of the carbody, and the direction of $\boldsymbol{F}'$ is always opposed to the lateral movement of the carbody. Hence, the vector relationship between $\boldsymbol{F}_y'$ and $\boldsymbol{T}_y'$ is obtained (Fig. 10), and Re and Im in Fig. 10 represent the real and imaginary parts in the complex plane, respectively.

As Fig. 10a shows, the phase lag between $\boldsymbol{F}_y'$ and $\boldsymbol{T}_y'$ is greater than 90° for the locomotive with OI layout, which would make the phase lag between the lateral and yaw motions of the carbody increase with the increase of A_{csx}. In Fig. 10b, when the OO layout is adopted in the locomotive, the phase lag between $\boldsymbol{F}_y'$ and $\boldsymbol{T}_y'$ is smaller than 90°, which is beneficial to reducing the phase lag between the lateral and yaw motions of the carbody with the increase of A_{csx}. For SS and ASS layouts, there are no additional torques, so the value of A_{csx} has little effect on the phase lag between the lateral and yaw motions of the carbody. Consequently, the influence of yaw damper layouts on the difference in lateral ride comfort between the front and rear ends of the carbody is perfectly explained.

7 Conclusions

1. This study describes the low-conicity/high-conicity stability Pareto optimization for high-speed locomotives (Bo-Bo) under four types of yaw damper layouts through the genetic algorithm NSGA-II, which is conducted based on the MATLAB/SIMPACK co-simulation platform. Then, the optimal lateral dynamics performance and suspension parameters matching relationship for locomotives under the four layouts are obtained. They provide a helpful comparison solution for bogie structure schemes, and can eliminate the interference of the matching relationship between suspension parameters and structural schemes in the results.

2. Based on the LHS using Monte Carlo simulations, the GSA for lateral ride comfort and operation safety performance of the locomotives under four yaw damper layouts to the six key suspension parameters has been conducted through the RBF-HDMR method. The following conclusions are important.

(1) Lateral ride comfort of the carbody on the straight track under the low-conicity condition is mostly sensitive to the yaw damper damping C_{sx} and lateral installation angle A_{csx}, and the influence of A_{csx} is more obvious when the OI or OO layout is adopted. This means the yaw damper layout has a significant effect on the lateral ride comfort on straight tracks.

(2) Operational safety on curved tracks is sensitive to yaw damper damping C_{sx} and primary lateral stiffness K_{py}, especially the former, but has little sensitivity to the value of A_{csx}, which indicates that yaw damper layouts have little effect on curve passing performance.

(3) When the locomotive adopts the OO layout, there is an interesting phenomenon that the value of A_{csx} is positively correlated with the value of W_{yf}, but is negatively related to the value of W_{yr}, which means that a moderate A_{csx} can reduce or even eliminate the difference in lateral ride comfort between the front and rear ends of the carbody. This is the unique characteristic of the locomotive with OO layout, and the value of A_{csx} is positively correlated with values of W_{yf}

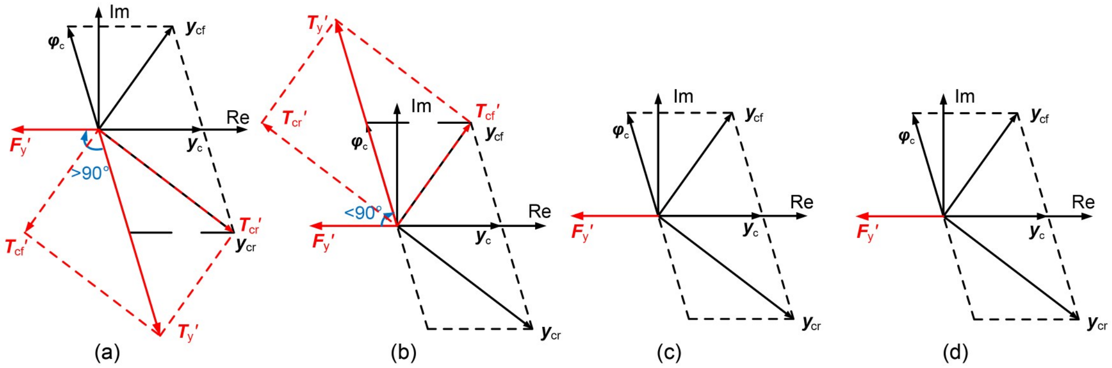

Fig. 10 Vector relationships of lateral additional forces and torques: (a) OI; (b) OO; (c) SS; (d) ASS

and W_{yr} for those locomotives with the other three layouts.

3. When the yaw damper layout has a lateral installation angle A_{csx}, the relative lateral displacement between the carbody and bogie frame will cause a certain deformation at both ends of the yaw damper, resulting in additional forces and torques. Based on this phenomenon, taking the whole carbody as the research object, a force analysis is conducted to explain the matching relationship between the yaw damper layout and A_{csx}. In addition, from the perspective of modal analysis, the influence mechanism of the layouts on the difference in lateral ride comfort between the front and rear ends of the carbody has also been given, and the selection principle of A_{csx} is pointed out when the locomotive adopts the four layouts.

Acknowledgments

This work is supported by the National Railway Group Science and Technology Program (Nos. N2020J026 and N2021J028) and the Independent Research and Development Project of State Key Laboratory of Traction Power, China (No. 2022TPL_Q02).

Author contributions

Guang LI and Yuan YAO designed the research. Longjiang SHEN and Xiaoxing DENG processed the corresponding data. Guang LI wrote the first draft of the manuscript. Wensheng ZHONG helped to organize the manuscript. Guang LI revised and edited the final version.

Conflict of interest

Guang LI, Yuan YAO, Longjiang SHEN, Xiaoxing DENG, and Wensheng ZHONG declare that they have no conflict of interest.

References

Alfi S, Mazzola L, Bruni S, 2008. Effect of motor connection on the critical speed of high-speed railway vehicles. *Vehicle System Dynamics*, 46(S1):201-214. https://doi.org/10.1080/00423110801935814

Bigoni D, True H, Engsig-Karup AP, 2014. Sensitivity analysis of the critical speed in railway vehicle dynamics. *Vehicle System Dynamics*, 52(S1):272-286. https://doi.org/10.1080/00423114.2014.898776

Chen XW, Yao Y, Shen LJ, et al., 2022. Multi-objective optimization of high-speed train suspension parameters for improving hunting stability. *International Journal of Rail Transportation*, 10(2):159-176. https://doi.org/10.1080/23248378.2021.1904444

ERRI (European Rail Research Institute), 1989. Application of the ISO2631 Standard to Railway Vehicle, ISO 2631. ERRI, Utrecht, the Netherlands.

Goldberg DE, 1989. Genetic Algorithms in Search, Optimization and Machine Learning. Addison-Wesley Professional, Boston, USA.

IUR (International Union of Railways), 1994. Guidelines for Evaluating Passenger Comfort in Relation to Vibration in Railway Vehicle, UIC Code 513. IUR, Paris, France.

Jeon CS, Kim YG, Park JH, et al., 2016. A study on the dynamic behavior of the Korean next-generation high-speed train. *Proceedings of the Institution of Mechanical Engineers, Part F: Journal of Rail and Rapid Transit*, 230(4): 1053-1065. https://doi.org/10.1177/0954409715576355

Jiang YZ, Wu PB, Zeng J, et al., 2020. Multi-parameter and multi-objective optimisation of articulated monorail vehicle system dynamics using genetic algorithm. *Vehicle System Dynamics*, 58(1):74-91. https://doi.org/10.1080/00423114.2019.1566557

Johnsson A, Berbyuk V, Enelund M, 2012. Pareto optimisation of railway bogie suspension damping to enhance safety and comfort. *Vehicle System Dynamics*, 50(9):1379-1407. https://doi.org/10.1080/00423114.2012.659846

Kalker JJ, 1982. A fast algorithm for the simplified theory of rolling contact. *Vehicle System Dynamics*, 11(1):1-13. https://doi.org/10.1080/00423118208968684

Kassa E, Nielsen JCO, 2008. Stochastic analysis of dynamic interaction between train and railway turnout. *Vehicle System Dynamics*, 46(5):429-449. https://doi.org/10.1080/00423110701452829

Li G, Wu RD, Deng XX, et al., 2022. Suspension parameters matching of high-speed locomotive based on stability/comfort Pareto optimization. *Vehicle System Dynamics*, 60(11):3848-3867. https://doi.org/10.1080/00423114.2021.1979602

Li JY, Liu LY, Kou DH, 2014. Wu Guang high-speed rail track irregularity power spectrum analysis. *Applied Mechanics and Materials*, 638-640:1224-1228. https://doi.org/10.4028/www.scientific.net/AMM.638-640.1224

Lyratzakis A, Tsompanakis Y, Psarropoulos PN, 2022. Mitigation of high-speed trains vibrations by expanded polystyrene blocks in railway embankments. *Journal of Zhejiang University-SCIENCE A (Applied Physics & Engineering)*, 22(1):6-20. https://doi.org/10.1631/jzus.A1900680

Mousavi-Bideleh SM, Berbyuk V, 2016a. Global sensitivity analysis of bogie dynamics with respect to suspension components. *Multibody System Dynamics*, 37(2):145-174. https://doi.org/10.1007/s11044-015-9497-0

Mousavi-Bideleh SM, Berbyuk V, 2016b. Multiobjective optimisation of bogie suspension to boost speed on curves. *Vehicle System Dynamics*, 54(1):58-85. https://doi.org/10.1080/00423114.2015.1114655

Mousavi-Bideleh SM, Berbyuk V, Persson R, 2016. Wear/comfort Pareto optimisation of bogie suspension. *Vehicle System Dynamics*, 54(8):1053-1076. https://doi.org/10.1080/00423114.2016.1180405

Pålsson BA, Nielsen JCO, 2012. Track gauge optimisation of

railway switches using a genetic algorithm. *Vehicle System Dynamics*, 50(S1):365-387.
https://doi.org/10.1080/00423114.2012.665167

Persson R, Andersson E, Stichel S, et al., 2014. Bogies towards higher speed on existing tracks. *International Journal of Rail Transportation*, 2(1):40-49.
https://doi.org/10.1080/23248378.2013.878294

Polach O, 2006a. Comparability of the non-linear and linearized stability assessment during railway vehicle design. *Vehicle System Dynamics*, 44(S1):129-138.
https://doi.org/10.1080/00423110600869537

Polach O, 2006b. On non-linear methods of bogie stability assessment using computer simulations. *Proceedings of the Institution of Mechanical Engineers, Part F: Journal of Rail and Rapid Transit*, 220(1):13-27.
https://doi.org/10.1243/095440905X33251

Shan SQ, Wang GG, 2010. Metamodeling for high dimensional simulation-based design problems. *Journal of Mechanical Design*, 132(5):051009.
https://doi.org/10.1115/1.4001597

Shao S, Zhang KL, Yao Y, et al., 2022. Investigations on lubrication characteristics of high-speed electric multiple unit gearbox by oil volume adjusting device. *Journal of Zhejiang University-SCIENCE A (Applied Physics & Engineering)*, 23(12):1013-1026.
https://doi.org/10.1631/jzus.A2200274

Shojaeefard MH, Khalkhali A, Yarmohammadisatri S, 2017. An efficient sensitivity analysis method for modified geometry of Macpherson suspension based on Pearson correlation coefficient. *Vehicle System Dynamics*, 55(6):827-852.
https://doi.org/10.1080/00423114.2017.1283046

Simpson TW, Booker AJ, Ghosh D, et al., 2004. Approximation methods in multidisciplinary analysis and optimization: a panel discussion. *Structural and Multidisciplinary Optimization*, 27(5):302-313.
https://doi.org/10.1007/s00158-004-0389-9

SAMR (State Administration for Market Regulation of the People's Republic of China), 2019. Specification for Dynamic Performance Assessment and Testing Verification of Rolling Stock, GB/T 5599-2019. National Standards of the People's Republic of China (in Chinese).

Sun JF, Chi MR, Jin XS, et al., 2021. Experimental and numerical study on carbody hunting of electric locomotive induced by low wheel–rail contact conicity. *Vehicle System Dynamics*, 59(2):203-223.
https://doi.org/10.1080/00423114.2019.1674344

Tao GQ, Liu XL, Wen ZF, et al., 2021. Formation process, key influencing factors, and countermeasures of high-order polygonal wear of locomotive wheels. *Journal of Zhejiang University-SCIENCE A (Applied Physics & Engineering)*, 22(1):70-84.
https://doi.org/10.1631/jzus.A2000081

Tunga MA, Demiralp M, 2005. A factorized high dimensional model representation on the nodes of a finite hyperprismatic regular grid. *Applied Mathematics and Computation*, 164(3):865-883.
https://doi.org/10.1016/j.amc.2004.06.056

Wang WL, Huang Y, Yang XJ, et al., 2011. Non-linear parametric modelling of a high-speed rail hydraulic yaw damper with series clearance and stiffness. *Nonlinear Dynamics*, 65(1-2):13-34.
https://doi.org/10.1007/s11071-010-9871-7

Wang WL, Yu DS, Huang Y, et al., 2014. A locomotive's dynamic response to in-service parameter variations of its hydraulic yaw damper. *Nonlinear Dynamics*, 77(4):1485-1502.
https://doi.org/10.1007/s11071-014-1393-2

Xia ZH, Zhou JS, Gong D, et al., 2020. Theoretical study on the effect of the anti-yaw damper for rail vehicles. *Proceedings of the Institution of Mechanical Engineers, Part C: Journal of Mechanical Engineering Science*, 234(2):457-473.
https://doi.org/10.1177/0954406219878752

Xu L, Zhai WM, Gao JM, 2018. Global sensitivity analysis for vehicle-track interactions: special attention on track irregularities. *Journal of Computational and Nonlinear Dynamics*, 13(3):031007.
https://doi.org/10.1115/1.4038820

Yan Y, Zeng J, 2018. Hopf bifurcation analysis of railway bogie. *Nonlinear Dynamics*, 92(1):107-117.
https://doi.org/10.1007/s11071-017-3634-7

Yan Y, Zeng J, Huang CH, et al., 2019. Bifurcation analysis of railway bogie with yaw damper. *Archive of Applied Mechanics*, 89(7):1185-1199.
https://doi.org/10.1007/s00419-018-1475-6

Yao Y, Zhang HJ, Luo SH, 2015. The mechanism of drive system flexible suspension and its application in locomotives. *Transportation*, 30(1):69-79.
https://doi.org/10.3846/16484142.2013.785977

Yao Y, Li G, Wu GS, et al., 2020. Suspension parameters optimum of high-speed train bogie for hunting stability robustness. *International Journal of Rail Transportation*, 8(3):195-214.
https://doi.org/10.1080/23248378.2019.1625824

Ye YG, Shi DC, Poveda-Reyes S, et al., 2020. Quantification of the influence of rolling stock failures on track deterioration. *Journal of Zhejiang University-SCIENCE A (Applied Physics & Engineering)*, 21(10):783-798.
https://doi.org/10.1631/jzus.A2000033

Zeng YC, Song DL, Zhang WH, et al., 2021. Stochastic failure process of railway vehicle dampers and the effects on suspension and vehicle dynamics. *Vehicle System Dynamics*, 59(5):703-718.
https://doi.org/10.1080/00423114.2019.1711136

Zhang H, Ran XR, Wang XG, et al., 2021. Coupling effects of yaw damper and wheel-rail contact on ride quality of railway vehicle. *Shock and Vibration*, 2021:6692451.
https://doi.org/10.1155/2021/6692451

Electronic supplementary materials

Table S1